

Analytic Characterization of the Wake Behind In-Stream Hydrokinetic Turbines

AUTHORS

Parakram Pyakurel
James H. VanZwieten
Florida Atlantic University

Tian Wenlong
Northwestern Polytechnical
University

Palaniswamy Ananthakrishnan
Indian Institute of Technology
Madras

Introduction

In-stream hydrokinetic turbines produce electrical power from rivers, tides, or ocean currents without impounding water through the use of dams. These turbines are placed directly in the flow field to generate electrical power from the kinetic energy of moving water (Johnson & Pride, 2010). Tidal turbine technologies have been advancing rapidly, with more than 40 new devices introduced between 2006 and 2013 (IRENA, 2014). Five different commercial types of marine turbine technologies, with turbine capacities ranging from 250 kW to 1 MW, have been successfully tested by several companies (Zhou et al., 2014). Also, full-scale deployments of single tidal turbines have been achieved (IRENA, 2014), and the first grid-connected in-stream hydrokinetic tidal turbine array is currently being installed, with the second of five 100-kW tidal turbines being installed in August of 2016 (Nova Innovation, 2016). Studies on impacts of the shape and density of tidal current arrays have been conducted

ABSTRACT

Analytical algorithms developed and optimized for quantifying the wake behind in-stream hydrokinetic turbines are presented. These algorithms are based on wake expressions originally developed for wind turbines. Unlike previous related studies, the optimization of empirical coefficients contained in these algorithms is conducted using centerline velocity data from multiple published experimental studies of the wake velocities behind in-stream hydrokinetic turbine models or porous disks and not using computational fluid dynamics. Empirical coefficients are first individually optimized based on each set of experimental data, and then empirically based coefficient expressions are created using all of the data sets collectively, such that they are functions of ambient turbulence intensity. This expands the applicability of the created algorithms to cover the expected range of operating conditions for in-stream hydrokinetic turbines. Wind turbine wake model expressions are also modified to characterize the dependence of wake velocities on radial location from the centerline of in-stream hydrokinetic turbines. Thus, expressions with empirically optimized coefficients for calculating wake velocities behind in-stream hydrokinetic turbines are described in terms of both centerline and radial positions. Wake predictions made using the Larsen model for radial dependence are shown to diverge from experimental measurements near the wake radius defined by the Jensen model, suggesting that this is a good indication of the cutoff point beyond which numerical estimations no longer apply. Results suggest that using a combined Larsen/Ainslie approach or combined Jensen/Ainslie approach for characterizing wake have similar mean errors to using only a Larsen approach.

Keywords: in-stream hydrokinetic turbine, marine energy converters, turbine wakes, turbulence intensity, velocity deficit

in the Severn Estuary and Bristol Channel (Ahmadian & Falconer, 2012) in order to understand the performance of turbines in an array setting.

Power production of in-stream hydrokinetic turbine arrays will be dependent on the effect that upstream turbine wakes have on downstream turbines. However, the impact of device spacing on array performance is not yet well understood (Uihlein & Maganga, 2016). Therefore, quantifying the wake behind a single turbine is

an important step in understanding array performance and optimizing device placement within an array. Experimental studies have shown that the mean wake velocity along the centerline (center of rotor) can be reduced to about 20% of freestream velocity at a location 2 diameters downstream of a single rotor, subsequently recovering to about 80% of the freestream value at a distance of 10 diameters downstream and to near freestream value (about 90% recovery) at 20 diameters downstream (Stallard et al., 2013).

However, wake recovery cannot be generalized because of its dependence on ambient turbulence intensity (TI; Hansen et al., 2012), with velocity recovering more quickly at higher ambient TIs (Bahaj et al., 2007; Blackmore et al., 2014; Maganga et al., 2010; Mycek et al., 2014). This is because higher ambient turbulence levels increase the mixing between different downstream flows velocities, leading to a more homogeneous mean wake field.

Although there are very limited models specifically created for predicting the wake behind river, tidal, or ocean current turbines, several models such as the Jensen, Larsen, Frandsen, and Ainslie wake models (Jensen, 1983; Larsen, 1988; Frandsen et al., 2006; Ainslie, 1988) do exist for predicting mean wake velocity behind wind turbines. These models contain analytic expressions that predict time-averaged far-wake velocities as a function of downstream centerline distance (Jensen, Larsen, and Frandsen models; Jensen, 1983; Larsen, 1988; Frandsen et al., 2006), as well as radial distance from centerline (Larsen and Ainslie models; Larsen, 1988; Ainslie, 1988). These analytical expressions contain coefficients that were either determined based on wind farm measurements or through wind tunnel studies.

The far-wake region is the area where the specific geometry and operating characteristics of a device no longer greatly impact the wake field (Vermeer et al., 2003). The properties of a rotor such as number of blades, blade aerodynamics, three-dimensional (3D) effects, and the tip vortices are pronounced in near wake, whereas modeling the actual rotor is less important for far wake (Vermeer et al., 2003). Therefore, numerical methods such as 3D Navier Stokes Solver have

been used in combination with an actuator line concept that uses tabulated airfoil data to account for the influence of rotating blades on the flow field to analyze near wake (Sorenson & Shen, 2002). However, the influence of rotating blades is negligible for the far-wake analysis, and therefore, simplified analytical models can be utilized. Several analytical far-wake models utilized for wind turbine are discussed in Wake Models section.

It has been suggested that for downstream distances beyond about 5 diameters, the wake field can be estimated using far-wake assumptions (Annoni et al., 2014). Experimental and numerical analyses have been carried out that study near and far-wake evolution supporting this transition distance (Javaherchi et al., 2014). Since this work is concerned with the impact of wake in farm situations, wake expressions discussed here that are only valid for the far-wake region are appropriate as downstream turbine spacing will be greater than this distance. Major parameters to impact far-wake velocity are freestream velocity, ambient TI, and thrust coefficient (Bahaj et al., 2007).

Multiple studies have been conducted to retune wind turbine wake models for the prediction of in-stream hydrokinetic turbine generated wakes. These studies have used computational fluid dynamics (CFD) generated profiles of wakes behind in-stream hydrokinetic turbines for coefficients tuning and algorithm validation (Palm et al., 2010; Gebreslassie et al., 2013; Brutto et al., 2015; Pyakurel et al., 2017). Although these studies provide some level of CFD model validation using measured data, they could introduce biases associated with CFD modeling into the analytic model tuning process. Additionally, only two

of these studies address the dependence of wake velocity on radial location (Palm et al., 2010; Pyakurel et al., 2017), and only one accounts for the dependence of wake propagation on freestream TI (Brutto et al., 2015). Fortunately, as the number of experimental wake studies increase, so does the ability to retune model coefficients using experimental data alone. The emerging availability of multiple experimental results also provides the opportunity to account for ambient TI in wake predictions, enabling developed models to predict wake fields over a wide range of operating conditions. This study, therefore, directly tunes wind turbine wake models using experimental in-stream hydrokinetic data, removing potential biases associated with CFD modeling. It also evaluates multiple wind turbine modeling approaches, allowing for the selection of the most appropriate algorithm, and accounts for TI in coefficient tuning to allow for broad applicability of the created algorithm. Finally, this study matches centerline wake models with those that account for radial location to create new wake modeling solutions.

Three wind turbine wake models are described in Wake Models section that can be used to calculate centerline velocity deficit and wake radius. The empirical coefficients in these models, which can be optimized for calculating centerline velocity deficit behind in-stream hydrokinetic turbines, are also shown. Then, expressions for expanding these algorithms to also describe the wake as a function of radial distance from the centerline are created for in-stream hydrokinetic turbines by modifying an existing wind turbine wake model. Coefficient Optimization for Centerline Velocity Deficit section utilizes results from multiple

experimental studies that measure centerline wake velocity deficit behind an in-stream hydrokinetic device to optimize the empirical coefficients in each of the wind turbine wake models. The optimized empirical coefficients are then utilized to calculate centerline wake velocity deficit behind an in-stream hydrokinetic device and compared with experimentally measured results. The dependence of the optimized empirical coefficients on ambient TI is then examined. Three approaches are presented in Full Wake Expression Analyses section, Larsen/Larsen, Jensen/Ainslie, and Larsen/Ainslie, for calculating wake velocities at radial distance from the centerline. Finally, Conclusions section draws conclusions based on these analyses.

Wake Models

Wake models for characterizing in-stream hydrokinetic turbine wake at centerline and radial locations are discussed in this section. Studies of wake that utilize numerical methods such as Large Eddy Simulation (Churchfield et al., 2015) and Blade Element Model (Masters et al., 2015) are also available, but are not considered here, as the motive of this paper is to develop computationally fast and inexpensive analytic equations to predict wake velocity. First, three wind wake models along with their empirical coefficients are presented for quantifying the centerline (downstream from the rotor center) wake velocity deficit and wake radius for the far field (≥ 5 rotor diameters). Next, two analytic expressions for predicting velocity deficit in the far-wake region as a function of radial location are presented. Together these form analytic expressions that define the

mean far field wake behind an in-stream hydrokinetic turbine, with coefficients that can be optimized using experimental in-stream hydrokinetic turbine wake field data.

Models for Centerline Velocity Deficit

Three models originally developed to characterize wake by centerline velocity deficits are considered in this study. These are the Jensen (1983), Larsen (1988), and Frandsen (Frandsen et al., 2006) models. Each of these models assumes the wake to be axisymmetric.

Jensen Centerline Model

N.O. Jensen (1983) developed expression for wake behind a wind turbine, neglecting near field and treating wake as a negative jet. Distance downstream up to which the near field effects exist was not explicitly stated, but near field was described as a field where swirling vortices make a special contribution (Jensen, 1983). The mean centerline wake velocity is calculated by the Jensen model as

$$V_x = U_o \left(1 - 2a \left(\frac{r_o}{r_o + \alpha x} \right)^2 \right), \quad (1)$$

where V_x is the centerline velocity at a downstream distance x , U_o is free-stream velocity, r_o is the radius of rotor, α is an empirical coefficient (generally taken as 0.01 for wind turbines), and a is the axial induction factor. This equation was obtained by assuming linear expansion of wake with x and by considering mass and momentum balances. For the velocity distribution in radial location, Jensen (1983) states that the velocity distribution “appears to be more Gaussian or bell shaped,” but no numerical charac-

terization was done and a simple top-hat distribution was assumed.

An expression relating axial induction factor to thrust coefficient, C_T , can be rewritten from the version presented in Hansen (2008) as

$$a = 1 - \sqrt{\frac{1 - C_T}{2}}. \quad (2)$$

From Equations 1 and 2, the centerline wake velocity deficit, U_c , can be calculated according to

$$U_c^* = 1 - \frac{V_x}{U_o} = \frac{(1 - \sqrt{1 - C_T})}{\left(1 + \frac{\alpha x}{r_o}\right)^2}. \quad (3)$$

Wake radius is a radius of axisymmetric wake at which the wake velocity approximately reaches the freestream velocity. The Jensen model defines the wake radius, r_x , as

$$r_x = r_o + \alpha x. \quad (4)$$

If velocity deficits at different distances downstream, thrust coefficient, and rotor diameter are available from experiments for in-stream hydrokinetic devices, α can be optimized to best fit the available experimental data sets. The simplicity and accuracy of the Jensen model could be reasons for its popularity in the wind industry. This model is the base of the Park model that was developed for wind farm calculations for the Wind Atlas Analysis and Application Program (WAsP), which is widely used for the estimation of wind resources (Peña et al., 2015). The Jensen model was also utilized to derive analytical expressions for a turbine farm layout consisting of six turbines (Gebreslassie et al., 2013). However, those expressions were derived for a new type of cross-flow

turbine known as Momentum Reversal Lift by Gebreslassie et al. (2013), whereas the expressions utilized in this paper are for a horizontal axis turbine.

Larsen Centerline Model

An analytic expression for turbine wake was also developed by Larsen (1988). The Larsen model assumed Prandtl's turbulent boundary layer equations and considered the mean wake flow as incompressible, stationary, and axisymmetric. The centerline velocity deficit obtained by setting the radial distance to zero in this expression is

$$U_c^* = 1 - \frac{V_x}{U_o} = \frac{1}{9} (C_T A_d x^{-2})^{\frac{1}{3}} \left(\left(\frac{35}{2\pi} \right)^{\frac{3}{10}} (3c_1^2)^{-\frac{1}{3}} \right)^2, \quad (5)$$

where A_d is rotor area, c_1 is nondimensional mixing length (empirical coefficient), and C_T is thrust coefficient.

The wake radius r_x is expressed as

$$r_x = \left(\frac{35}{2\pi} \right)^{\frac{1}{3}} (3c_1^2)^{\frac{1}{3}} (C_T A_d x)^{1/3}. \quad (6)$$

The coefficient c_1 in Equation 5 can be optimized so that the calculated wake behind in-stream hydrokinetic turbines best match experimental data if the centerline velocity deficit at different distances downstream, thrust coefficient, and rotor area are available from experiments.

Frandsen Centerline Model

Analytical expressions for the wind speed deficit in wind farms was also described analytically by Frandsen et al. (2006). The centerline wake velocity deficit is calculated using this approach according to Frandsen et al. (2006):

$$U_c^* = 1 - \frac{V_x}{U_o} = \frac{1}{2} \pm \frac{1}{2} \sqrt{1 - \frac{2A_d C_T}{A_w}}, \quad (7)$$

where A_w and A_d are wake area and rotor swept area, respectively.

To decide whether the “+” or “-” sign will be used in the above equation, wake induction factor a' is defined as

$$a' = 1 - \frac{U'_w}{U_o}, \quad (8)$$

where U'_w is flow speed in the wake just after the initial wake expansion and U_o is freestream velocity of fluid. For $a' \leq 0.5$, “-” is used, and for $a' > 0.5$, “+” sign is used.

The Frandsen model defines wake radius r_x according to

$$r_x = \left(\beta^{\frac{k}{2}} + \alpha' s \right)^{1/k} r_o, \quad (9)$$

where $k = 3$ if the Schlichting solution as recommended in Frandsen et al. (2006) is chosen, r_o is the rotor radius, $s = \frac{x}{2r_o}$, α' is an empirical coefficient to be

determined experimentally, and β is given by

$$\beta = \frac{1}{2} \frac{1 + \sqrt{1 - C_T}}{\sqrt{1 - C_T}}. \quad (10)$$

In order to most accurately use the Frandsen model to characterize the mean centerline wake deficit behind an in-stream hydrokinetic turbine, the coefficient α' can be optimized by best fitting the calculated wake deficit to available experimental data sets. Initially, β can be calculated using Equation 10 for known C_T . Then, r_x can be calculated using Equation 9 for different values of α' . The wake area A_w is then calculated as πr_x^2 . This wake area is utilized in Equation 7 to calculate centerline velocity deficit. Finally, the calculated centerline velocity can be compared with experimentally measured centerline velocity deficit to optimize α' .

All the models discussed above have empirical coefficients determined from experimental studies for wind turbines. By using experimental studies for in-stream hydrokinetic turbines, these coefficients can be optimized for in-stream hydrokinetic turbines.

Models for Radial Dependence of Velocity Deficit

The Jensen and Frandsen wake models were developed to estimate the mean centerline velocity deficit alone, whereas the Larsen model can be applied to predict the velocity deficit as a function of both downstream and radial location (Equation 15). Therefore, the Larsen model is directly utilized to predict wake velocity as a function of downstream and radial location. Additionally, equations from the Ainslie (1988) model are modified to estimate velocity deficit

as a function of radial location, when centerline velocity data from the algorithms presented in Models for Centerline Velocity Deficit section are utilized.

Ainslie Radial Model

Ainslie (1988) described a numerical model that can be used to calculate the time-averaged wake flow field using time-averaged Navier-Stokes equations for incompressible flow with eddy viscosity closure (Ainslie, 1988). This approach neglects pressure gradient in wake field and assumes Gaussian profile for the wake velocity dependence on radial position. For 2 diameters downstream, velocity deficit at different radial positions was given by Ainslie (1988) as

$$1 - \frac{U_w}{U_o} = U_{\text{deficit}}^* e^{\left(-3.56\left(\frac{r^*}{b}\right)^2\right)}, \quad (11)$$

where U_{deficit}^* is the centerline velocity deficit at 2 diameters downstream, r^* is radial distance coordinate (from wake centerline) that has been made non-dimensional by dividing radial distance by rotor diameter, b is wake width parameter, and U_w^* is wake velocity corresponding to nondimensional radial coordinate r^* .

The wake width parameter, b , in Equation 11 was calculated from conservation of momentum as

$$b = \left[\frac{3.56C_T}{8U_{\text{deficit}}^*(1 - 0.5U_{\text{deficit}}^*)} \right]^{1/2}. \quad (12)$$

The Ainslie model was set up to solve the Navier-Stokes equations numerically by making use of Equation 11 for a centerline distance 2 diameters downstream. However, in this study, Equations 11 and 12 are written as a function of centerline

velocity and therefore can be used for any centerline distance that is within the far-wake region.

To form mathematical expressions for calculating normalized wake velocity (U_w/U_o) behind in-stream hydrokinetic turbines, Equations 11 and 12 are modified as

$$\frac{U_w}{U_o} = 1 - U_c^* e^{\left(-3.56\left(\frac{r}{2r_o b}\right)^2\right)}, \quad (13)$$

where,

$$b = \left[\frac{3.56C_T}{8U_c^*(1 - 0.5U_c^*)} \right]^{1/2}; \quad (14)$$

r is the radial distance from turbine centerline; U_c^* is the centerline wake velocity deficits obtained from other wake models such as Jensen, Larsen, and Frandsen through Equations 3, 6, and 7, respectively; and U_w is wake velocity for a location defined by r and x . Because U_c^* is a function of downstream distance, results found using Equations 13 and 14 will vary with downstream distance when calculating the normalized velocity as a function of radial location. It is noteworthy that Equation 13 defines a Gaussian profile for the far-wake region, which is consistent with observations that the far-wake region can be approximated as following a Gaussian profile (Jensen, 1983; Sande et al., 2011).

Larsen Radial Model

The Larsen model can be used to predict wake velocity deficit as a function of both downstream distance and radial location. However, it is suggested that this equation be applied only for radial distance lower than wake radius defined in Equation 6 (Larsen, 1988). A simplified version of this equation for calculating wake velocity deficit along the centerline is presented in Equation 5, with the wake velocity calculated using the Larsen model as a function of both downstream and radial location described according to

$$\frac{U_w}{U_o} = 1 - \frac{1}{9} (C_T A_d x^{-2})^{\frac{1}{3}} \left(r^{\frac{3}{2}} (3c_1 C_T A_d x)^{-\frac{1}{2}} - \left(\frac{35}{2\pi} \right)^{\frac{3}{10}} (3c_1^2)^{-\frac{1}{5}} \right)^2. \quad (15)$$

Coefficient Optimization for Centerline Velocity Deficit

Empirical coefficients α , c_1 , and α' (see Models for Centerline Velocity Deficit section) from Jensen, Larsen, and Frandsen models, respectively, are optimized to calculate centerline velocity deficits that best match experimentally measured centerline velocity deficit data for in-stream hydrokinetic turbines operating in flows with different ambient TI values. Then, expressions that calculate these coefficients as a function of TI are presented. Finally, coefficients obtained from the presented expressions are utilized to calculate centerline wake velocity deficit and compared with experimentally published results in this section.

Coefficient Optimization for Each TI

Several experimental studies have been conducted to quantify the centerline wake velocity deficits behind in-stream hydrokinetic turbines using small-scale tidal turbine models or porous disks (Blackmore et al., 2014; Maganga et al., 2010; Neary et al., 2013; Mycek et al., 2014). Nine different data sets containing experimentally measured centerline velocity deficits presented by Blackmore et al. (2014), Maganga et al. (2010), Neary et al. (2013), and Mycek et al. (2014) are used to optimize the empirical coefficients of wake models discussed in Models for Centerline Velocity Deficit section. These experimentally measured centerline velocity deficits are measured in flows with the following nine TI values: 3%, 4%, 5%, 7%, 8%, 9.8%, 11%, 14%, and 15%. For every TI, all of the available centerline velocity deficits for downstream distances of 5 diameters and beyond are utilized, with the interval and farthest distance as published (Blackmore et al., 2014; Maganga et al., 2010; Neary et al., 2013; Mycek et al., 2014) to optimize model coefficients α (Jensen model), c_1 (Larsen model), and α' (Frandsen model).

Coefficient optimizations are carried out by minimizing the root mean square error (*rmse*) defined as

$$rmse = \sqrt{(U_m^* - U_c)^2}, \quad (16)$$

where U_m^* is experimentally measured velocity deficits (Blackmore et al., 2014; Maganga et al., 2010; Neary et al., 2013; Mycek et al., 2014) and U_c^* is the vector of centerline velocity deficits calculated from wake models at corresponding downstream distances using Equations 3, 5, 7, and 9. An iterative search algorithm is utilized to

vary the individual model coefficients to minimize this error. Thus, optimized values of α , c_1 , and α' are obtained separately for each TI that best fit the range of available centerline velocity deficits 5 diameters downstream and beyond. The *rmse* is used as the optimization parameter because it emphasizes large deviations and we are trying to minimize the deviations between calculated values and experimental values. Also, *rmse* is a widely used metric in signal processing (Wang & Bovik, 2009), and this metric is more appropriate when the error distribution is expected to be Gaussian (Chai & Draxler, 2014).

Centerline Velocity Analyses for Coefficients Optimized at Each TI

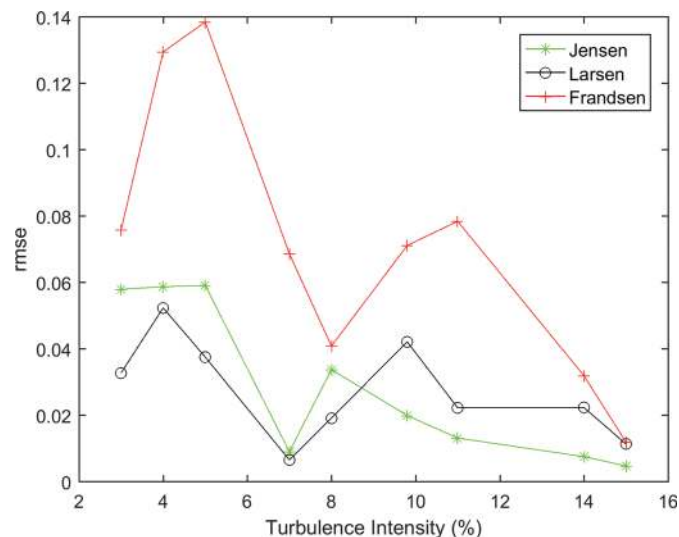
Centerline velocity deficits calculated using the coefficients separately optimized for each TI are compared with experimental results here. The *rmse* of centerline velocity deficit calculated using Equation 16 for the optimized coefficients associated with the Jensen, Larsen, and Frandsen models are shown in Figure 1. While evaluat-

ing the Frandsen model, the Schlichting solution is chosen (i.e., $k = 3$) as suggested in Frandsen et al. (2006). Furthermore, while evaluating the Frandsen model, monotonic expansion of the wake is assumed, and only the solution of $\alpha' \leq 0.5$ is considered in Equation 7 as the solution for $\alpha' \geq 0.5$ yields an imaginary component of centerline velocity deficit. It is found that Jensen and Larsen models with optimized α and c_1 both have lower *rmse* than the Frandsen model for each of the evaluated TIs (Figure 1).

The *rmse* averaged over the evaluated TI values for Jensen and Larsen models are found to be 0.029 and 0.027, respectively, suggesting that on average these models have similar accuracy. However, the *rmse* error averaged over TI values between 3% and 8% is 0.029 for the Larsen model, which is significantly less than the averaged *rmse* value of 0.043 obtained for Jensen model. On the contrary, for TI between 9.8% and 15%, the Larsen model has averaged *rmse* value of 0.024, which is more than twice the averaged *rmse* value of

FIGURE 1

Comparison of *rmse* values obtained when the wake model coefficients are tuned individually for each data set.



0.011 obtained for Jensen model. Furthermore, for each of the considered data sets in Blackmore et al. (2014), Maganga et al. (2010), Neary et al. (2013), and Mycek et al. (2014), both Jensen and Larsen models fit the experimental data set closer than the Frandsen model. A similar result has been documented for wind turbines (Andersen et al., 2014). Based on *rmse* values, the Larsen model is observed to have the greatest accuracy at lower ambient TI values (lesser or equal to 8%) whereas the Jensen model is found to have greatest accuracy at higher ambient TI values (greater than 8%).

To help visualize the accuracy of these models with optimal coefficients in predicting the centerline wake deficit over the evaluated far-wake region (≥ 5 rotor diameter), measured and calculated wake deficit for three TIs are presented (Figure 2). These experimentally measured velocity deficits are discussed in detail by Blackmore et al. (2014), Maganga et al. (2010), and Mycek et al. (2014). Centerline

downstream distance is normalized according to x/D , which is centerline downstream distance, x , divided by rotor diameter, D . Figure 1 is for ambient TI values of 3% (x/D ranges from 5 to 10), 8% (x/D ranges from 5 to 9), and 14% (x/D ranges from 5 to 15). Calculated velocities for TIs of 3% and 8% show larger *rmse* values than the calculated velocities for TI of 14%. Also, the rate of decrease of velocity deficit with downstream distance predicted by wake models is lower than experimental values for TIs of 3% and 8%. However, for TI of 14%, rate of decrease of velocity deficit with downstream distance predicted by the Jensen model is very close to experimental values. The other two models (Larsen and Frandsen) predicted a slower velocity deficit decay than experimentally measured values for each of these TIs.

The Reynolds number in the experimental setup of Mycek et al. (2014) is in the range of 0.28×10^6 and 0.84×10^6 . An experimental study (Bachant & Wosnik, 2014) of

crossflow hydrokinetic turbine has found that there is no significant dependence of near-wake velocity deficit on Reynolds number for the range of Reynolds numbers between 0.3×10^6 and 1.3×10^6 . However, Reynolds numbers could affect the far-wake characteristics, but this effect has not been considered in the current paper due to the lack of sufficient data that would allow the development of mathematical relationships between Reynolds number and coefficients of wake models.

Model Coefficient as a Function of TI

Dependence of optimized coefficients α and c_1 in the Jensen and Larsen models on ambient TI are examined in this section, and analytic expressions for calculating the Jensen and Larsen coefficients as a function of TI are presented. Coefficients from the Frandsen model are excluded from the evaluation because of the relatively high error associated with this model (see Centerline Velocity Analyses for Coefficients Optimized at Each TI section). The individually optimized (using Equation 16 for each TI) coefficients for Jensen and Larsen models are presented as a function of TI in Figure 3. The values of coefficients increase nonlinearly with TI, and it can be seen that these coefficients do not neatly follow low order curves (likely due to differences in experimental operating conditions, measurements noise, differences in measurement techniques, etc.) but do show some obvious basic trends. Dashed and dotted curves in Figure 3 represent expressions that best fit these data (discussed later).

Expressions for calculating model coefficients as a function of TI are developed to best fit data points for

FIGURE 2

Comparison of calculated and experimentally measured centerline velocity deficits for TIs of 3%, 8%, and 14% for different wake models.

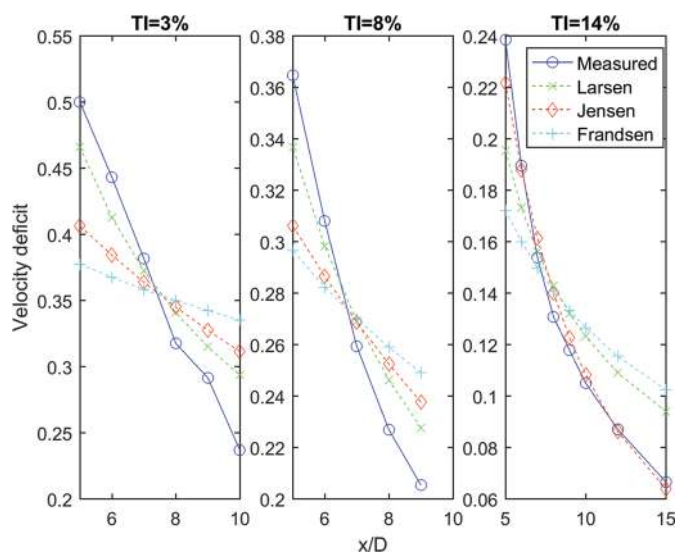
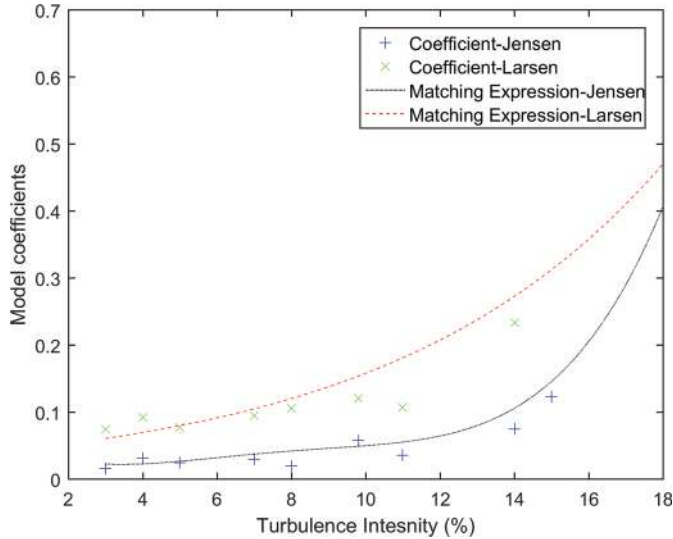


FIGURE 3

Calculated optimal Jensen and Larsen coefficients presented as a function of ambient TI.



the Jensen and Larsen models (Figure 3). It is assumed that values of coefficients increase with TI over the evaluated range, and therefore, only exponential and polynomial expressions that monotonically increase with TI from 3% to 15% are considered. Because only nine data points are available, polynomials of order up to 4 are considered even though polynomials higher than order 4 may have comparatively lesser R^2 value. Of the polynomial and exponential expressions, the equation with the highest R^2 value is selected.

Using abovementioned considerations, the following fourth-order polynomial is found to best relate the Jensen coefficient (α) to TI:

$$\alpha = 0.00003TI^4 - 0.0009TI^3 + 0.0097TI^2 - 0.0396TI + 0.0763, \quad (17)$$

with an R^2 value of 0.91.

It is noteworthy that a mathematical relationship between α and TI was also proposed by Brutto et al. (2015). However, the proposition of Brutto et al. was only for the Jensen model

whereas we have considered the Larsen and Frandsen models in addition to the Jensen model. Furthermore, the proposition of Brutto et al. (2015) was based on a CFD simulation, whereas the relationship proposed here (Equation 17) is based on nine different sets of previously published experimental studies as discussed in Coefficient Optimization for each TI section.

An exponential curve is found to best define the relationship between the Larsen coefficient and TI for the entire evaluated data range (TI range of 3–15%). The resulting exponential equation that best fits the Larsen coefficient is

$$c_1 = 0.0406e^{0.1361TI}, \quad (18)$$

with an R^2 value of 0.73. The dotted and dashed lines in Figure 2 represent Equations 17 and 18, respectively.

Centerline Algorithm Analysis for Coefficients Calculated as a Function of TI

To evaluate how accurately wake models with empirical coefficients calculated as a function of TI predict

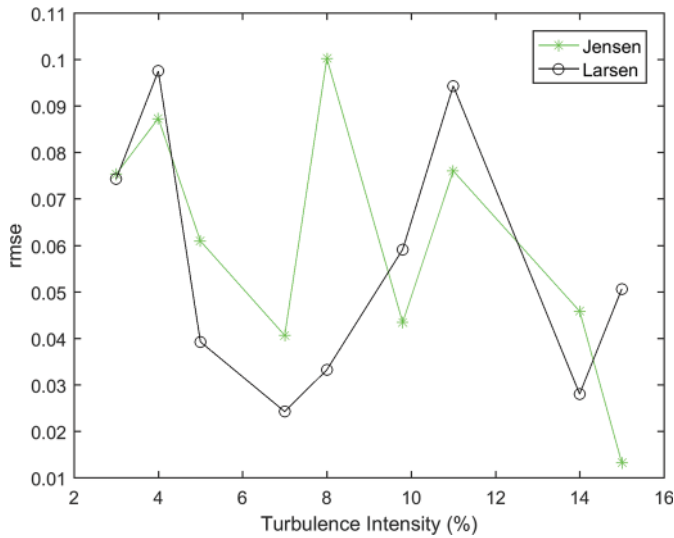
centerline velocity deficits, results obtained using these models are compared with the experimental measurements. Figure 4 shows $rmse$ predicted using the Jensen and Larsen wake models (Equations 3 and 5) with Equations 17 and 18 used to compute α and c_1 .

The $rmse$ averaged over TI for both the Jensen and Larsen models in Figure 4 are about two times higher than the corresponding $rmse$ values in Figure 1. Similar to the results from coefficients optimized for every TI (Figure 1), the Larsen model has a lower $rmse$ for lower TI, i.e., TI of 3%, 5%, 7%, and 8%. However, unlike the results presented in Figure 1, the Jensen model has a lower $rmse$ than the Larsen model at TI of 4% after using coefficients calculated from Equations 17 and 18. The difference could be due to the value of optimized Larsen coefficient being higher than Larsen coefficient calculated using Equation 18 for TI of 4% as seen in Figure 3.

Another common result seen in Figures 1 and 4 is that Jensen model has lower $rmse$ for higher TI, i.e., TI of 9.8%, 11%, and 15%. However, the Larsen model is found to have a lower $rmse$ than the Jensen model at TI of 14% in Figure 4, which is different from Figure 1. This difference could be caused by the value of the optimized Jensen coefficient for TI of 14% being lower than the coefficient obtained using Equation 17. However, the general trend that the Larsen model has low $rmse$ at lower TI and the Jensen model has low $rmse$ at higher TI is common to both Figures 1 and 4. The results using optimized coefficients presented in Figure 1 represent specific experimental and operating conditions, whereas results presented in Figure 4 using Equations 17 and

FIGURE 4

Comparison of *rmse* values using coefficients obtained from Equations 17 and 18.



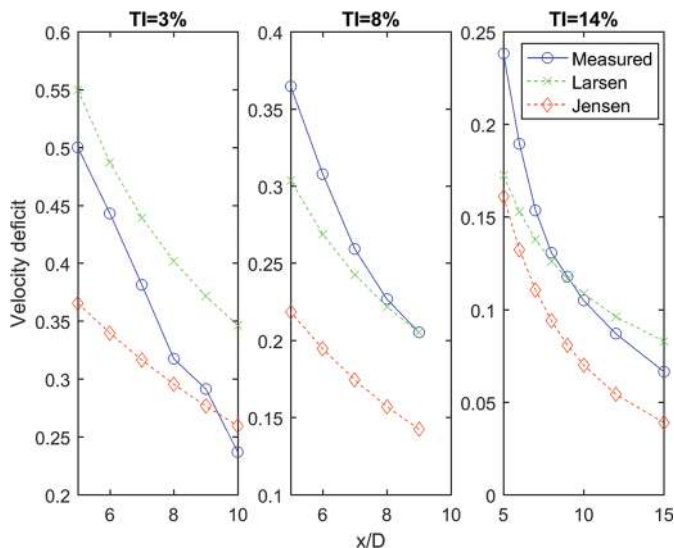
Equations 17 and 18 generalize wake predictions by averaging out the results of different experimental conditions. Therefore, application of Equations 17 and 18 to compute coefficients are likely to predict general centerline wake profile more accurately as the bias to specific experimental and operation conditions are minimized.

Figure 5 compares experimentally measured centerline velocity deficit

data for TI of 3%, 8%, and 14% with calculated data using Larsen and Jensen coefficients computed from Equations 17 and 18. It is noteworthy that wake propagation is not only dependent on TI but also on other experimental and operating conditions such as blockage ratio, current shear and tip speed ratio. The model coefficients based on Equations 17 and 18 represent a general case, whereas

FIGURE 5

Comparison of calculated and experimentally measured centerline velocity deficits for Jensen and Larsen models using Equations 17 and 18 to compute corresponding coefficients.



the coefficients based on Equation 16 represent an experimental setup specific case. Therefore, unless more complicated wake models are developed that include additional effects such as these, Equations 17 and 18 may often be better for general wake modeling than the coefficients optimized from a single experiment.

For the analytical expressions that calculate centerline velocity deficit as a function of TI (Equations 3 and 17 for Jensen model; Equations 5 and 18 for Larsen model), the Larsen model is found to best match the experimental data for TI range of 3% to 8% in terms of lowest average *rmse*, suggesting that Equations 5 and 18 are most suitable for TI up to and including 8%. Likewise, the Jensen model is found to be the best match for TI higher than 8% in terms of lowest average *rmse* from 9.8% to 15%. Therefore, the Jensen model (Equations 3 and 17) is most suitable for TI greater than 8%.

Full Wake Expression Analyses

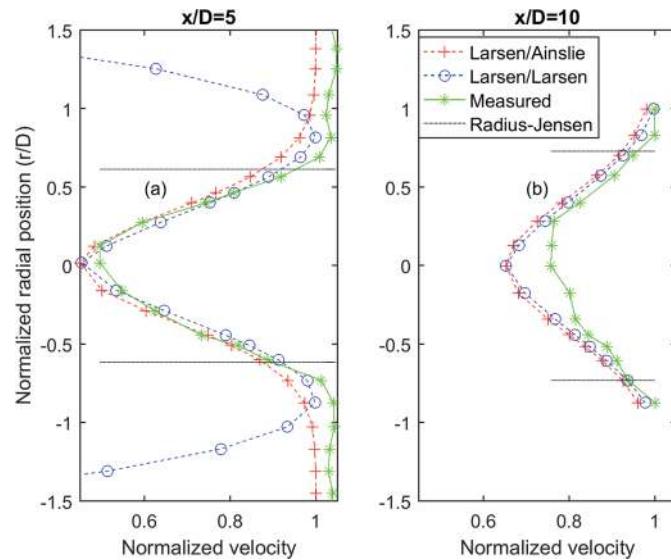
This section utilizes both the centerline and radial wake expressions in Wake Models section, with the coefficients calculated in Model Coefficient as a Function of TI section, to characterize wake velocity as a function of centerline distance and radial distance from centerline. Three approaches are used to calculate normalized wake velocities (normalized by dividing wake velocity by freestream velocity) as a function of both downstream and radial locations. Equations 13 and 14 adapted from the Ainslie model are used to calculate normalized wake velocities at radial locations using centerline velocity deficit obtained from the Jensen model (Equation 3)

to form the Jensen/Ainslie approach. Similarly, Equations 13 and 14 are used with centerline velocity deficit calculated from the Larsen model (Equation 5) to form the Larsen/Ainslie approach. The empirical coefficients α and c_1 required for calculating centerline velocities in the Jensen/Ainslie or Larsen/Ainslie approaches are obtained from Equations 17 and 18. For TI up to and including 8%, the Larsen/Ainslie approach is used in this section, whereas for TI greater than 8%, the Jensen/Ainslie approach is used. This is because the accuracy of Equations 13 and 14 in predicting wake velocities at radial locations is dependent on the accuracy of centerline velocity deficits plugged in these equations and, as previously mentioned, the Jensen model is more accurate for centerline velocity deficits greater than 8% whereas the Larsen model is more accurate for TI lesser than and including 8%. The third approach is to use the Larsen model for calculating normalized wake velocities as a function of both downstream and radial location (Equation 15) using the coefficient c_1 obtained from Equation 18. For the sake of naming consistency, this approach is referred here as the Larsen/Larsen approach.

Only two published data sets (three TIs; Maganga et al., 2010; Mycek et al., 2014) considered in this study contain wake velocity measurements at radial locations. Figure 6 compares the normalized wake velocities at radial locations calculated from the Larsen/Ainslie and Larsen/Larsen approaches, with experimentally measured velocities published in Mycek et al. (2014) for a TI of 3%. Centerline normalized distances of $x/D = 5$ (Figure 6a) and 10 (Figure 6b) are presented, with the radial distance also normalized using rotor diameter (r/D). These centerline

FIGURE 6

Comparison of Larsen/Larsen and Larsen/Ainslie approaches with measured velocity at radial locations for TI = 3%.



distances correspond to the approximate beginning of the far-wake region, as well as the farthest downstream location that was measured. It is noteworthy that both the Larsen/Ainslie and Larsen/Larsen approaches give the same normalized velocity at $r/D = 0$ because centerline velocity deficits are calculated using the same model (Larsen model). As radial distance increases, the normalized wake velocity is observed to increase with the lowest wake velocity observed at the centerline.

It can be seen in Figure 6 that the Larsen/Larsen approach does not monotonically increase as a function of radial location, whereas the Larsen/Ainslie (and Jensen/Ainslie) approach is a Gaussian equation that converges monotonically toward 1 as radial location increases. It is also noted that the Larsen/Larsen approach is closer to experimental values than Larsen/Ainslie for approximate radial distance (r/D) range of 0.55–0.65. Furthermore, it can be seen that normalized wake velocities calculated from approaches presented here diverge significantly from the measured values beyond r/D

of approximately 0.6–0.8. This limitation in wake approaches could be due to assumptions regarding relationship between wake radius (r_x) and downstream centerline distance (x) in wake models. For example, Jensen models assume r_x to be proportional to x whereas Larsen models assume r_x to be proportional to $x^{1/3}$. It is also noteworthy that only the Larsen model (called here as the Larsen/Larsen approach for naming consistency) is originally formulated to calculate wake velocity at radial position. Jensen/Ainslie and Larsen/Ainslie approaches are formed here by modifying and combining the Ainslie model with the Larsen or Jensen model. Another reason for the divergence in calculated and experimental wake velocities at radial location could be due to variation in turbulence levels at different radial positions, with turbulence being highest at the center. Because of this divergence, it is important to establish a radial cutoff location where the accuracy of wake approaches can be compared quantitatively, and more importantly, establish a radial

distance beyond which these approaches should not be utilized. For this, wake radii are used.

Wake radii are used in the development of the Jensen (Equation 4), Larsen (Equation 6), and Frandsen (Equation 9) models to define the control volume used to develop wake velocity expressions inside this region. These radii were calculated using Equations 4 and 6 by substituting the values of corresponding coefficients obtained from Equations 17 or 18. By comparing wake radii of different models, it was found (this analysis is not shown here for brevity) that the wake radius calculated from the Jensen model best describes a cutoff point beyond which experimentally measured data start to diverge from calculated data for Jensen/Ainslie, Larsen/Ainslie, and Larsen/Larsen approaches. For the Jensen/Ainslie or Larsen/Ainslie approach, this divergence results from the actual water velocity often exceeding the freestream values shortly after this cutoff point, as the equations from the Ainslie model (Equation 13) defines a Gaussian curve which converges towards freestream velocity but never exceeds it. For the Larsen/Larsen approach, this divergence is because the utilized expression (Equation 15) is not monotonic and the normalized wake velocity starts to decrease shortly after the cutoff point (see Figure 6a). Jensen wake radii for x/D of 5 and 9 (or 10) are shown in Figures 4–6 (dotted horizontal lines). The radii calculated using Equation 4 can be seen to provide a reasonable estimate for cutoff points beyond which the approaches presented in this paper cannot be applied to calculate normalized velocities.

For wake velocity data inside this cutoff range, $rmse$ values are utilized to compare calculated velocities with

experimentally measured velocities at each downstream distance. Here, $rmse$ is calculated using the measured and analytical expressions at equally spaced radial distances from the centerline to the wake radius. Thus, this $rmse$ is different from the $rmse$ mentioned in Equation 16. For TI of 3%, the $rmse$ value averaged over the two centerline distances of 5 and 10 diameters (Figure 6) for the Larsen/Ainslie approach and Larsen/Larsen approach are found to be 0.053 and 0.045, respectively. In this case the Larsen/Larsen approach is slightly more accurate, as can be seen in Figure 6.

Figure 7 compares normalized velocities obtained from Larsen/Ainslie and Larsen/Larsen approaches with experimentally measured velocities published in Maganga et al. (2010) within the Jensen wake radius for a TI of 8%. The centerline distances of $x/D = 5$ (Figure 7a) and 9 (Figure 7b) are shown. For this TI, the average $rmse$ value averaged over these two centerline distances for the Larsen/Ainslie

approach and Larsen/Larsen approach are found to be 0.034 and 0.038, respectively. Unlike the results for a TI of 3%, these results suggest that the Larsen/Ainslie approach is slightly more accurate.

Figure 8 compares normalized velocities obtained from Jensen/Ainslie and Larsen/Larsen approaches with experimentally measured velocities published in Mycek et al. (2014) for a TI of 15%. The centerline distances of $x/D = 5$ (Figure 8a) and 10 (Figure 8b) are shown. By comparing Figures 6, 7, and 8, it can be seen that normalized wake velocity at a given centerline distance increase with increase in TI. It is also observed that the Gaussian wake profile is more prominent at lower TI.

For TI of 15%, the average $rmse$ value for the Jensen/Ainslie approach is slightly more accurate than the Larsen/Larsen approach with $rmse$ values of 0.038 and 0.047, respectively. Like previous cases, only data points up to the Jensen wake radius are taken to calculate $rmse$, and the Jensen wake

FIGURE 7

Comparison of Larsen/Larsen and Larsen/Ainslie approaches with measured velocity at radial locations for TI = 8%.

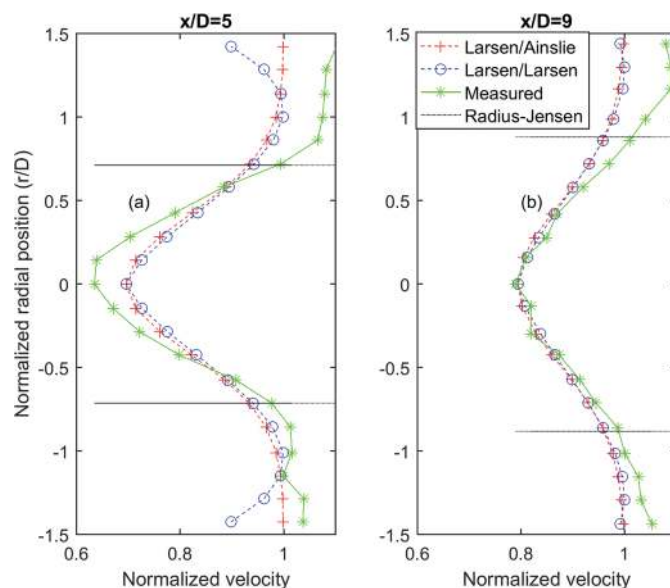
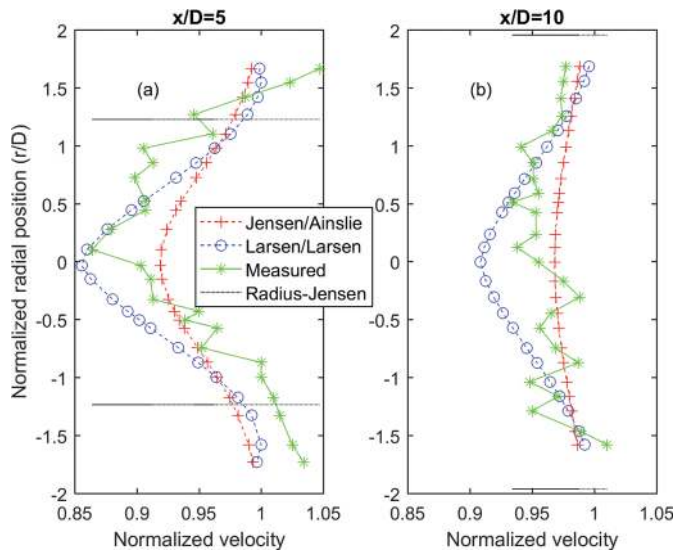


FIGURE 8

Comparison of Larsen/Larsen and Jensen/Ainslie approaches with measured velocity at radial locations for TI = 15%.



radius appears to be a reasonable approximation for where the approaches presented in this paper and measurements diverge. The reason that Figure 8 looks different than Figures 6 and 7 is likely due to noise in the experimentally measured data in Figure 8. It is noteworthy that normalized velocity predictions from the Jensen/Ainslie and Larsen/Larsen approaches converge as radial distance increases. This could be because both these approaches tend to make the value of normalized wake velocity 1 as radial distance increases up to and slightly beyond the cutoff point marked by radius from Jensen model.

It is found that the TI averaged (3, 8, and 15%) *rmse* of the Larsen/Larsen approach is 0.043, and this value for Larsen/Ainslie (or Jensen/Ainslie depending on TI) approach is 0.042. Therefore, it can be said that the Larsen/Larsen approach and combined Jensen/Ainslie or Larsen/Ainslie approach give similar wake velocity predictions over the evaluated radial range, with Larsen/Ainslie or Jensen/Ainslie approach performing only

marginally better. For TI of 3%, the Larsen/Larsen approach is found to match the experimentally measured data slightly better, whereas for TI of 8% and 15%, Larsen/Ainslie (or Jensen/Ainslie depending on TI) approach is found to be slightly better in terms of lower *rmse* value. Only three different values of TI are considered because radial wake profiles were not available for the other TIs.

These results also suggest that the Jensen/Ainslie or Larsen/Ainslie may be slightly more accurate than the Larsen/Larsen approach near the beginning of the far-wake region; i.e., 5D downstream (Figures 6a–8a) for TI of 3% and 8%. The TI averaged *rmse* of the Larsen/Larsen approach and Jensen/Ainslie or Larsen/Ainslie approach for $x/D = 5$ are 0.043 and 0.041, respectively.

The experimentally measured as well as the calculated results show that the placement of a turbine in free-stream flow fields causes wake velocity to be less than freestream up to certain radial locations. After this radius, the wake velocity attains freestream veloc-

ity and often continues to increase slightly beyond the freestream value. This can be seen in Figures 6–8 where the normalized velocity is slightly greater than 1 (by 2–3%) at radial location higher than wake radius in experimentally measured results. The increased flow region can increase the power output of downstream devices slightly above their freestream power output if the array layout is optimized which has been previously highlighted (Myers & Bahaj, 2011). In such conditions, wake velocity starts to decelerate after reaching certain maximum value and eventually again becomes equal to freestream velocity. This is the radial point where the effect of placement of turbine/obstruction to the flow is not felt; i.e., the point where there is no wake effect. The presented equations do not capture this increased flow region and therefore this study is limited to velocity prediction at radial locations up to the wake radius.

Conclusions

Coefficients of the Jensen, Larsen, and Frandsen wind turbine wake models are optimized to calculate centerline wake velocity deficits behind in-stream hydrokinetic turbines. This optimization is done using a search algorithm that varies these coefficients to minimize *rmse* between model calculated centerline wake velocity deficits and experimentally measured centerline wake velocity deficits published for in-stream hydrokinetic turbines. The Jensen and Larsen models are found to best predict the centerline flow velocity behind in-stream hydrokinetic turbines after optimizing their coefficients over different TI ranges. These optimized coefficients are shown to be a function of ambient TI and mathematical

expressions relating the coefficients and TI are proposed. The coefficients could also be a function of the Reynolds number, which can be considered in future studies to further tune the optimal values of the coefficients. For lesser TI values (up to and including 8%), the Larsen model is observed to have the highest accuracy, whereas the Jensen model is found to have highest accuracy for TI greater than 8% for the experimental data sets considered in this study.

Calculated centerline wake velocity deficits from the Jensen (TI greater than 8%) or Larsen (TI up to and including 8%) model are then used with equations modified from the Ainslie model to form the Jensen/Ainslie or Larsen/Ainslie approach. Also, the Larsen model is used to calculate normalized wake velocities at radial locations to form Larsen/Larsen approach. The empirical coefficients (α and c_1) utilized in these approaches to calculate centerline velocity deficits are obtained from proposed TI-dependent expressions (Equations 17 and 18). These approaches are used to calculate normalized wake velocities as a function of both centerline and radial locations. These approaches are found to be approximately equally accurate for predicting normalized wake velocities at different radial locations up to a radial distance defined by the Jensen wake radius.

Acknowledgments

We would like to thank the National Science Foundation and specifically the Energy, Power, Control and Networks program for their valuable ongoing support in this research within the framework of grant ECCS-1307889 “Collaborative Research: Optimized Harvesting of Hydrokinetic

Power by Ocean Current Turbine Farms Using Integrated Control.”

Corresponding Author:

Parakram Pyakurel
Florida Atlantic University
Email: ppyakurel2014@fau.edu

References

- Ahmadian**, R., & Falconer, R.A. 2012. Assessment of array shape of tidal stream turbines on hydro-environmental impacts and power output. *Renew Energ.* 44(2012):318-27. <https://doi.org/10.1016/j.renene.2012.01.106>.
- Ainslie**, J. 1988. Calculating the flowfield in the wake of wind turbines. *J Wind Eng Ind Aerod.* 27:213-24. [https://doi.org/10.1016/0167-6105\(88\)90037-2](https://doi.org/10.1016/0167-6105(88)90037-2).
- Andersen**, S.J., Sørensen, J.N., Ivanell, S., & Mikkelsen, R.F. 2014. Comparison of engineering wake models with CFD simulations. *J Phys Conf Ser.* 524(2014):012161. <https://doi.org/10.1088/1742-6596/524/1/012161>.
- Annoni**, J., Seiler, P., Johnson, K., Fleming, P., & Gebraad, P. 2014. Evaluating wake models for wind farm control. American Control Conference, June 4–6, Oregon, USA. <https://doi.org/10.1109/ACC.2014.6858970>.
- Bachant**, P., & Wosnik, M. 2014. Reynolds number dependence of cross flow turbine performance and near-wake characteristics. Proceedings of the 2nd Marine Energy Technology Symposium. METS 2014, April 15–18, 2014, Seattle, WA.
- Bahaj**, A.S., Myers, L.E., Thomson, M.D., & Jorge, N. 2007. Characterising the wake of horizontal axis marine current turbines. Proceedings of the 7th European Wave and Tidal Energy Conference, Porto, Portugal, 2007.
- Blackmore**, T., Batten, W.M.J., & Bahaj, A.S. 2014. Influence of turbulence on the wake of a marine current turbine simulator. *Proc R Soc A.* 470(2170):20140331. <https://doi.org/10.1098/rspa.2014.0331>.
- Brutto**, O.A.L., Nguyen, V.T., Guillou, S.S., Gualous, H., & Boudart, B. 2015. Reanalyse of an Analytical Model for One Tidal Turbine Wake Prediction. Proceedings of the 11th European Wave and Tidal Energy Conference, Nantes, France.
- Chai**, T., & Draxler, R.R. 2014. Root mean square error (RMSE) or mean absolute error (MAE)?—Arguments against avoiding RMSE in the literature. [Online]: <http://www.geosci-model-dev-discuss.net/7/C473/2014/gmdd-7-C473-2014-supplement.pdf> (Last accessed on March 22, 2017).
- Churchfield**, M.J., Li, Y., & Moriarty, P.J. 2015. A large-eddy simulation study of wake propagation and power production in an array of tidal-current turbines. *Philos T R Soc A.* 371:2012042. <http://dx.doi.org/10.1098/rsta.2012.0421>.
- Frandsen**, S., Barthelmie, R., Pryor, S., Rathmann, O., Larsen, S., Højstrup, J., ... Thøgersen, M. 2006. Analytical modelling of wind speed deficit in large offshore wind farms. *Wind Energ.* 9(1-2):39-52. <http://dx.doi.org/10.1002/we.189>.
- Gebreslassie**, M.G., Belmont, M.R., & Tabor, G.R. 2013. Comparison of analytical and CFD modelling of the wake interactions of tidal turbines. Proceedings of the 10th European Wave and Tidal Energy Conference, Denmark.
- Hansen**, K.S., Barthelmie, R.J., Jensen, L.E., & Somme, A. 2012. The impact of turbulence intensity and atmospheric stability on power deficits due to wind turbine wakes at Horns Rev wind farm. *Wind Energ.* 2012; 15:183-96. <https://doi.org/10.1002/we.512>.
- Hansen**, M.O.L. 2008. Aerodynamics of wind turbines. Sterling, VA: Earthscan, pp. 31-3.
- IRENA Ocean Energy Technology Brief 3.** 2014. Tidal Energy: Technology Brief,” IRENA. http://www.irena.org/DocumentDownloads/Publications/Tidal_Energy_V4_WEB.pdf (accessed July 2, 2016).
- Javaherchi**, T., Stelzenmuller, N., Seydel, N., & Aliseda, A. 2014. Experimental and numerical analysis of a scale-model horizontal axis hydrokinetic turbine. Proceedings of the 2nd

Marine Energy Technology Symposium. METS 2014, April 15–18, 2014, Seattle, WA.

Jensen, N. 1983. A note on wind generator interaction. Risø National Laboratory, Roskilde, Denmark, pp. 5-7.

Johnson, J.B., & Pride, D.J. 2010. River, tidal, and ocean current hydrokinetic energy technologies: Status and future opportunities in Alaska. Alaska Energy Authority. http://www.uaf.edu/files/acep/2010_11_1_State_of_the_Art_Hydrokinetic_Final.pdf (accessed July 2, 2016).

Larsen, G. 1988. A Simple Wake Calculation Procedure. Risø National Laboratory, Roskilde, Denmark, pp. 22-6.

Maganga, F., Germain, G., King, J., Pinon, G., & Rivoalen, E. 2010. Experimental characterisation of flow effects on marine current turbine behaviour and on its wake properties. *IET Renew Power Gen.* 4(6):498-509. <https://doi.org/10.1049/iet-rpg.2009.0205>.

Masters, I., Williams, A., Croft, T.N., Togneri, N., Edmunds, M., Zangiabadi, E., ... Karunarathna, H. 2015. A comparison of numerical modelling techniques for tidal stream turbine analysis. *Energies.* 8(8):7833-53. <http://dx.doi.org/10.3390/en8087833>.

Mycek, P., Gaurier, B., Germain, G., Pinon, G., & Rivoalen, E. 2014. Experimental study of the turbulence intensity effects on marine current turbines behaviour, Part I: One single turbine. *Renew Energ.* 66:729-46. <https://doi.org/10.1016/j.renene.2013.12.036>.

Myers, L.E., & Bahaj, A.S. 2011. An experimental investigation simulating flow effects in first generation marine current energy converter arrays. *Renew Energ.* 37:28-36. <https://doi.org/10.1016/j.renene.2011.03.043>.

Neary, V.S., Gunawan, B., Hill, C., & Chamorro, L.P. 2013. Near and far field flow disturbances induced by model hydrokinetic turbine: ADV and ADP comparison. *Renew Energ.* 60:1-6. <https://doi.org/10.1016/j.renene.2013.03.030>.

Nova Innovation. 2016. Shetland Tidal Array. Available: <http://www.novainnovation.com/tidal-array>. Accessed: Jan 31, 2017.

Palm, M., Huijsmans, R., Pourquie, M., & Sijtsma, A. 2010. Simple wake models for tidal turbines in farm arrangement. Proceedings of the ASME 29th International Conference on Ocean, Offshore and Arctic Engineering, OMAE 2010, Shanghai, China. <https://doi.org/10.1115/OMAE2010-20966>.

Peña, A., Réthoré, P.E., & van der Laan, M.P. 2015. On the application of the Jensen wake model using a turbulence-dependent wake decay coefficient: The Sexbierum case. *Wind Energ.* 19(4):763-76. <http://dx.doi.org/10.1002/we.1863>.

Pyakurel, P., Tian, W., Van Zwieten, J.H., & Dhanak, M. 2017. Characterization of the mean flow field in the far wake region behind ocean current turbines. *J Ocean Eng Mar Energ.* 3(2):113-23. <https://doi.org/10.1007/s40722-017-0075-9>.

Sanderse, B., van der Pijl, S.P., & Koren, B. 2011. Review of computational fluid dynamics for wind turbine wake aerodynamics. *Wind Energ.* 14:799-819. <https://doi.org/10.1002/we.458>.

Sorenson, J.N., & Shen, W.Z. 2002. Numerical Modeling of Wind Turbine Wakes. *J Fluids Eng.* 124(2):393-9. <http://dx.doi.org/10.1115/1.1471361>.

Stallard, T., Collings, R., Feng, T., & Whelan, J.I. 2013. Interaction between tidal turbine wakes: Experimental study of a group of 3-bladed rotors. *Philos T R Soc A.* 371(1985). <http://dx.doi.org/10.1098/rsta.2012.0159>.

Uihlein, A., & Maganga, D. 2016. Wave and tidal current energy—A review of the current state of research beyond technology. *Renew Sust Energy Rev.* 58:1070-81. <https://doi.org/10.1016/j.rser.2015.12.284>.

Vermeer, L.J., Sorensen, J.N., & Crespo, A. 2003. Wind turbine wake aerodynamics. *Prog Aerosp Sci.* 39:467-510. [https://doi.org/10.1016/S0376-0421\(03\)00078-2](https://doi.org/10.1016/S0376-0421(03)00078-2).

Wang, Z., & Bovik, A.C. 2009. Mean squared error: Love it or leave it? A New Look at Signal Fidelity Measures. *IEEE Signal Proc Mag.* 26(1): 98-117. Available at: https://ece.uwaterloo.ca/~z70wang/publications/SPM09_figures.pdf.

Zhou, Z., Scullier, F., Charpentier, J.F., Benbouzid, M., & Tang, T. 2014. An up-to-date review of large marine tidal current turbine technologies. In: *Power Electronics and Application Conference (Shanghai; 2014)*, China. <https://doi.org/10.1109/PEAC.2014.7037903>.